Astron. Astrophys. 329, 571–578 (1998)

ASTRONOMY
AND
ASTROPHYSICS

Insights into the accretion flow in QS Telescopii (RE1938-461) from HST observations⋆

D. de Martino[1], **M. Mouchet**[2,3], **S.R. Rosen**[4], **B.T. Gänsicke**[5], **K.L. Clayton**[4], **and K.O. Mason**[4]

[1] Osservatorio Astronomico di Capodimonte, Via Moiariello 16, I-80131 Napoli, Italy
[2] DAEC, Observatoire de Paris, Section de Meudon, F-92195 Meudon Cedex, France
[3] University Denis Diderot, Place Jussieu, F-75005 Paris, France
[4] Department of Physics and Astronomy, University of Leicester, University Rd., Leicester, LE1 7RH, UK
[5] Universitäts Sternwarte, Geismarlandstr. 11, D-37083 Göttingen, Germany

Received 4 April 1997 / Accepted 19 August 1997

Abstract. We present HST/FOS observations of the polar QS Tel (RE1938-461) revealing new details in its 140 min UV orbital variability. A colour-dependent continuum orbital modulation as well as a narrow dip in its light curve, occurring at the same orbital phases as the one detected in the EUVE band, are observed. Their spectral dependence allows us to identify the heated regions of the white dwarf surface with complex structure and temperature gradients as well as the accretion stream. The absorption dip occurs during the minimum of UV emission line light curves and is interpreted as the occultation of the heated spot on the white dwarf surface by the accretion stream. We also confirm the strong UV modulation of the emission lines which, in these high time resolved spectroscopic data, is structured and consistent with X-ray irradiation of the stream material.

Key words: stars: cataclysmic variables – ultraviolet: stars – stars: individual: QS Tel

1. Introduction

AM Her stars or Polars, are a subgroup of magnetic Cataclysmic Variables (mCVs) which contain a low mass main sequence star transferring material to a synchronously rotating magnetized (B$\sim$ 10-230 MG) white dwarf. The accretion flow is dominated by the magnetic field of the white dwarf and is channelled towards its magnetic polar regions where a standing shock is produced above the white dwarf surface. The hot post-shock plasma emits hard X-rays, partially absorbed and re-emitted from the surface in the soft X-rays and EUV range, as well as cyclotron emission which is observed at optical and IR wavelengths (see review by Cropper 1990).

The Polar QS Tel/RE1938-461 was discovered during the ROSAT All Sky Survey in both soft X-rays (Beuermann & Thomas 1993) and the EUV (Buckley et al. 1993) being the brightest EUV emitting AM Her star detected. With a period of 140 min, QS Tel was also the first AM Her system discovered in the 2-3hr CV period gap. QS Tel is variable on timescales of months showing changes in its luminosity level as well as variations in its accretion pattern, the flow apparently switching from one accreting pole to a two pole accretion configuration (Buckley et al. 1993; Schwope et al. 1995; Rosen et al. 1996). However the relation between these two types of variable behaviour is not known yet. This system is one of the most interesting since optical observations have revealed that the main accreting pole facing the donor star (primary pole), has a lower field than the second pole (Schwope et al. 1995). Furthermore QS Tel is found to display an absorption dip in its soft X-ray and EUV orbital light curves, attributed to the occultation of the main pole of the white dwarf by the accretion stream (Rosen et al. 1996).

This system is also a bright UV source (de Martino et al. 1995). UV line fluxes and radial velocities were found to be strongly modulated at the orbital period and were proposed to be formed in the magnetically confined accretion stream. On the other hand, the far UV continuum flux only appeared to be weakly modulated in the IUE data. This was interpreted as a contribution from the heated white dwarf surface. Higher time resolved UV spectroscopy than achieved with IUE is then necessary to probe temporal features such as the absorption dip and the possible occurrence of a double-humped light curve, as observed in the EUVE data. In particular, only for a few systems has orbitally resolved UV spectroscopy been obtained at different levels of accretion and, hence, it is still an open question whether the second accretion pole is bright in the UV.

Here we present the first HST/FOS observations of QS Tel which reveal detailed structural characteristics in the UV range allowing us to examine the contributions of different emission regions.

Send offprint requests to: D. de Martino

⋆ Based on observations collected with the NASA/ESA Hubble Space Telescope, obtained at the Space Telescope Science Institute

Table 1. Journal of observations.

Slot #	Date	UT_{start} hh:mm	Duration s	$\phi^*_{start} - \phi^*_{end}$
1	1994 June 27	20:11	327	0.206 – 0.242
2	1994 June 27	21:04	1501	0.582 – 0.758
3	1994 June 27	21:34	1096	0.795 – 0.923
4	1994 June 27	22:41	2850	0.272 – 0.609
5	1994 June 28	00:17	1808	0.962 – 0.175
6	1994 June 28	00:52	808	0.213 – 0.307
7	1994 June 28	01:54	1000	0.653 – 0.769

* Adopting ephemeris from Schwope et al. (1995)

2. Observations and data reduction

HST Faint Object Spectrograph observations of QS Tel were performed on June 27/28 1994, after the COSTAR servicing mission and very close to one of the IUE observations reported by de Martino et al. (1995). The observations were carried out in the rapid mode, and spanned about 6hrs with a total effective on source exposure time of 9390 s. Due to the low-Earth HST orbit the observations were performed during 5 consecutive HST orbits, resulting in 7 continuous exposure slots as detailed in Table 1. The G160L grating was operated with the blue digicon covering the range 1154-2508 Å at a resolution of 6.8 Å diode^{-1} and with the 0.9" circular aperture (Kinney 1994). A total of 475 spectra were collected, each with an effective exposure time of $\sim$ 19s. The data were processed via the routine STScI pipeline, providing flux and wavelength calibrated spectra with the wavelength scale being accurate to $\sim$ 0.3 pixels ($\sim$ 2 Å or $\sim$ 400 km s^{-1} at 1550 Å).

The circular FOS 0.9" aperture in the blue digicon shows a flat-field feature at $\sim$ 1500 Å (Keys 1995) which affects the blue wing of the CIV line. This has been taken into account in the line analysis as detailed in Sect. 4.2.3

3. The FOS Spectrum of QS Tel

The average FOS UV spectrum of QS Tel (Fig. 1) is very similar in shape and flux level to that observed with IUE in 1993 and 1994 by de Martino et al. (1995) with a UV luminosity of $8 \cdot 10^{31}$ erg s^{-1} for an assumed distance of 170pc (the average value of 150-190 pc (Schwope et al.1995)). The typical UV emission lines seen in Polars (de Martino 1995) are also identified in the FOS spectrum as CIII λ1176, Lyα λ1216, NV λ1240, the blend of Si III λ1298/SiII λ1304/OI λ1305, CII λ1335, SiIV λ1397, CIV λ1550 (note the blue wing at λ 1505 due to the flat-field feature), HeII λ1640 and AlIII λ1855. The enhanced S/N of the FOS data compared with the IUE LWP spectra allows us to discern weak emission lines from CIII λ2297, HeII λ2307 and HeII λ2386. These lines are also observed in the HST FOS spectra of other mCVs (Stockman & Schmidt 1996; Silber et al. 1996). As it will be discussed in Sect. 4.1, and differently from IUE large aperture spectra, or from data taken with the HST FOS 4.3" aperture (Eracleous & Horne 1996), the Lyα geocoronal emission (FWHM =15.5 Å in our 0.9" spectra), does not dominate the observed emission line.

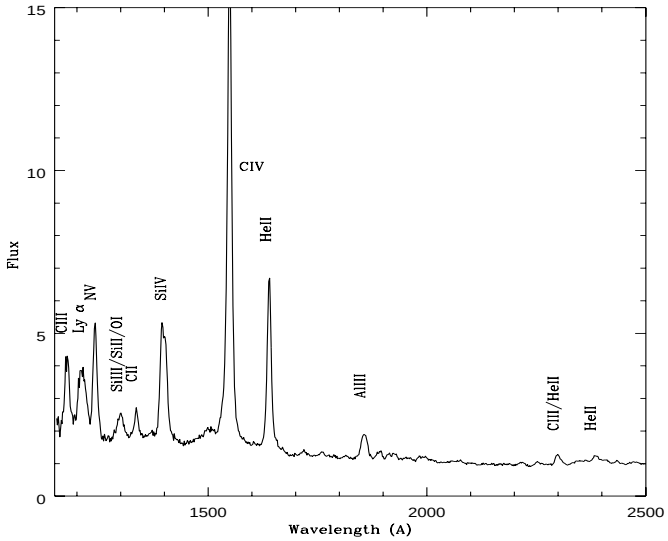

Fig. 1. The average UV spectrum of QS Tel. Ordinates are in units of 10^{-14} erg cm^{-2} s^{-1} Å $^{-1}$.

4. Temporal variability

UV variability has been investigated in both continuum and emission lines. Four broad band continuum fluxes have been measured for each spectrum in the ranges λ1260 – 1280, λ1420 – 1500, λ1710 – 1810 and λ1900 – 2500 for a time series analysis. Henceforth we will refer to these four bands as band 1, band 2, band 3 and band 4 respectively. However, for the study of UV continuum light curves in the far UV, we enlarged band 1 from λ 1250 to λ 1350 removing the Silicon/Oxygen blend and CIII emission, by means of Gaussian fits to the 200 orbital phase binned spectra (cfr. Sect. 4.2.). Fluxes in the main emission lines of Lyα, NV, SiIV, CIV and HeII have been measured adopting a method which uses for the continuum a power law distribution as found from a fitting procedure in the above continuum bands.

4.1. Time series analysis

A Fourier power spectrum analysis has been performed using the DFT algorithm of Deeming (1975). Due to the sampling of the HST data, governed by the HST orbit, we have also used the CLEAN algorithm of Roberts et al. (1987) adopting a gain 0.1 and 500 iterations. Both methods have been applied to the entire light curves of the total continuum flux, each continuum band and the emission line fluxes.

In Fig. 2, the UV continuum and emission line power spectra and their CLEANED spectra are shown. The major peak is observed at the well known 140 min orbital period, while its second harmonic is only observed in the emission line power spectra. Further peaks are also detected, partially reflecting the effect or aliasing of the 96 min HST orbit which are removed by

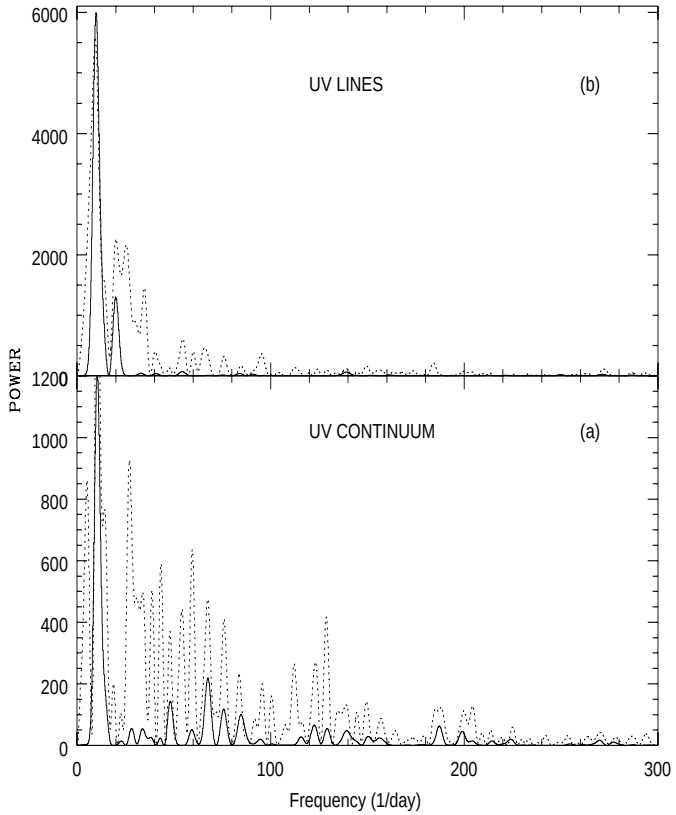

Fig. 2a and b. The power spectra of the total UV continuum (**a**) and UV lines (**b**) in QS Tel. The dirty and CLEANED spectra are shown with dashed and continuum lines respectively. Ordinates are in units of $(10^{-14}$ erg cm^{-2} s$^{-1})^2$. The strongest peak is at the orbital frequency 10.3 d^{-1}.

the CLEAN procedure. We also inspected the Lyα power spectrum for the presence of effects due to the geocoronal emission. While it is expected to be modulated at the 96 min HST orbit, our data do not show any variability at this frequency and therefore the Lyα emission is dominated by the intrinsic source contribution. This also means that the geocoronal component cannot be easily removed and hence any measure will only be an upper limit to the intrinsic contribution of the emission line.

The presence of the second harmonic in the emission lines is also confirmed by means of a sinusoidal fit to the observed light curves using the orbital and the second harmonic frequencies whose amplitudes result to be $1.60 \pm 0.06 \cdot 10^{-12}$ erg cm^{-2} s^{-1} and $9.55 \pm 0.04 \cdot 10^{-13}$ erg cm^{-2} s^{-1}. No second harmonic was necessary to fit the continuum light curve.

We have also searched for other significant peaks detrending the data of the low frequency variability by means of a 20-point smoothing function and recomputed the power spectra. Although in both line and continuum power spectra, peaks in the range of frequencies 1.1-3.3 mHz (15 min- 5 min) are present, they are found not to be statistically significant. However, variations of few percent on a timescale of few minutes are evident in the continuum and line light curves (see also Fig. 3). A cross-correlation analysis of the line and continuum data for the two longest segments, as composed by slot 4 and 5/6 (mostly continuous), shows that the continuum flickering only lags by ~ 30 s the emission line ones. Such variability, likely due to non periodic activity, is also observed in the optical (Schwope et al. 1995; Rosen et al. 1996).

4.2. Orbital variability

We have investigated the orbital behaviour of the UV emission in QS Tel by averaging the UV spectra in 200 orbital phase bins using the orbital ephemeris of Schwope et al. (1995) where they define phase zero as the inferior conjunction of the secondary star.

4.2.1. The continuum modulation

Light curves The UV continuum fluxes in the four bands defined in Sect. 4., have been measured for the 200 orbital phase binned spectra and the folded continuum light curves are presented in Fig. 3 (left side). Their shape is not smooth with a short term activity of a few percent on a timescale $\sim$ 10 min which, due to the short duration of our data set, does not fully average out.

The morphology in different bands is very similar, showing a single peaked quasi-sinusoidal modulation with a steeper rise and a slower decay. The maximum is relatively broad ranging between phase 0.1 and 0.4 (henceforth the bright phase), with a tendency to drift towards later phases at long wavelengths. In particular the near-UV (band 4) flux modulation reaches a maximum at $\sim$ 0.36. The minimum is found at phase 0.8 $\pm$ 0.1, henceforth the faint phase. These light curves are broadly compatible with lower temporal resolution IUE data (de Martino et al. 1995). The UV continuum modulation appears to be colour dependent, the variations being stronger in the far-UV. From sinusoidal fits the modulated fractions are 34$\pm$2% in band 1, 20$\pm$2% in band 2, 17$\pm$1% in band 3 and 19$\pm$2% in band 4.

Given the single peaked shape of the UV light curves we have compared the observed modulation with those observed with the ROSAT PSPC and WFC instruments during the All Sky Survey and during pointed observations in October 1992 when QS Tel was observed in one pole accretion mode (Buckley et al. 1993; Rosen et al. 1996). The phasing of the bright phases of both WFC and PSPC is $\sim$ 0.8-1.2, hence broader than and anticipating by 0.2 in orbital phase the UV maximum. Furthermore, the slow UV decay is not seen in the on-off behaviour of the WFC and PSPC light curves. Also, a lag by $\sim$ 0.1 in phase is found between the UV maximum and the primary maximum (between 0.93-1.26) of the double humped EUVE light curve when QS Tel was in a two pole accretion mode. This suggests that the UV emitting region(s) are not solely and simply associated with the ones observed at higher energies.

Furthermore, a dip superimposed on the bright phase is observed in all bands between phases $\sim$ 0.96 and 1.06. This range of the orbital cycle has been covered only once (Fig. 4). Although we cannot be certain of the repeatibility of this feature, it is roughly in phase with the EUVE dip observed between 0.97

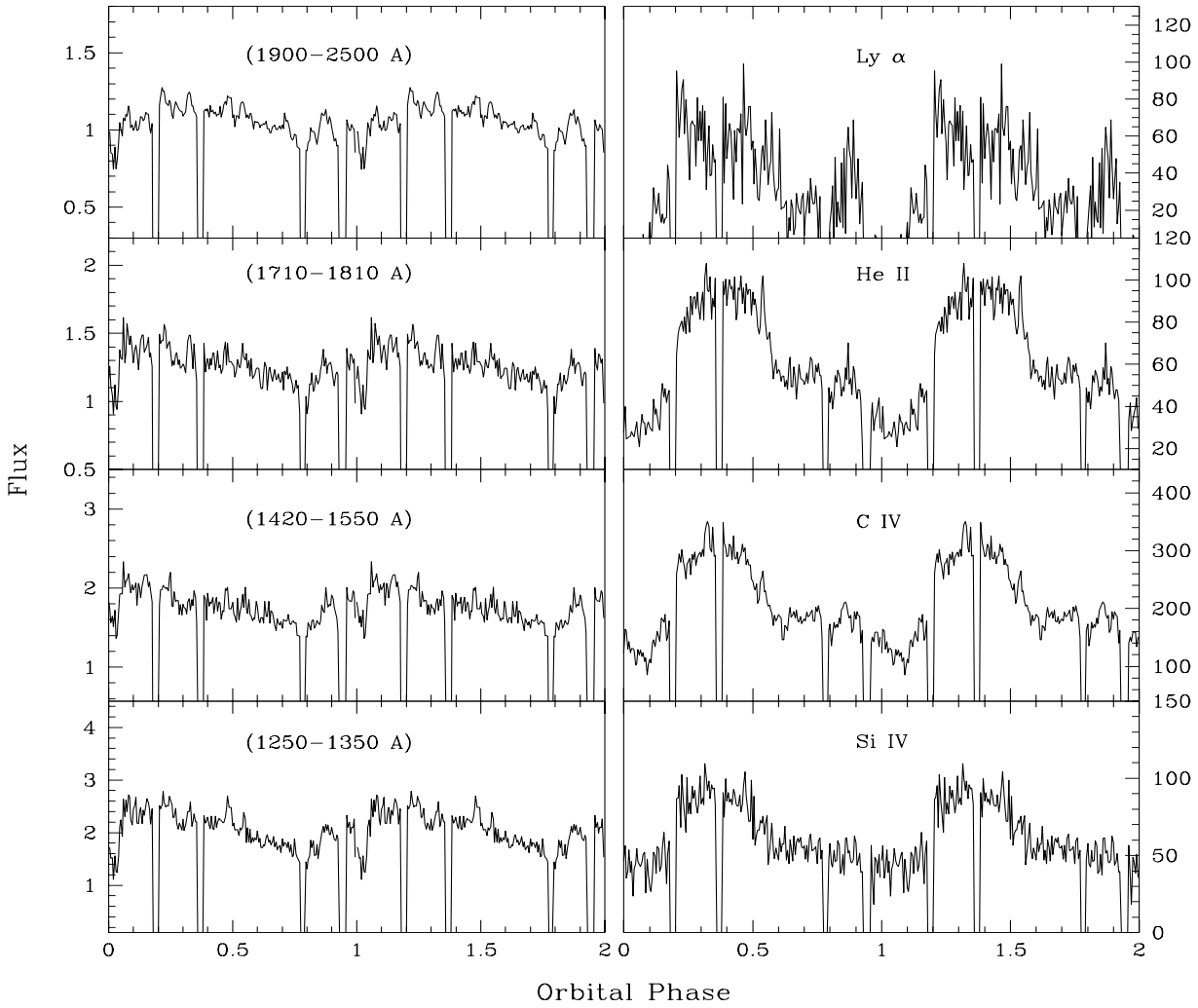

Fig. 3a and b. The UV continuum (**a**) and line flux (**b**) light curves. Average continuum fluxes in four selected bands together are in units of 10^{-14} erg cm^{-2} s^{-1} Å $^{-1}$. Lyα, HeII, CIV and SiIV line fluxes are in units of 10^{-14} erg cm^{-2} s^{-1}. Note the gaps due to the HST orbital sampling.

- 1.10 (Rosen et al. 1996), with a similar morphology: a relatively slow ingress and a faster egress. However the duration of the ingress is $\sim$ 500 s, while in the EUVE data it is $\sim$ 300 s and the egress is $\sim$ 210 s whilst the EUVE one lasts only 40 s suggesting that the UV emitting region has a less sharply defined edge. We also point out that the dip appears to be structured possibly due to flaring or enhanced absorptions. The dip appears to be colour dependent with depth fractions, defined with respect to the immediate post-dip phases, of 35±5% in band 1, 19±4% in band 2, 22±3% in band 3 and 16±2% in band 4.

Spectral shape In order to derive information on the nature of the continuum emission, we have analyzed the energy dependence of the UV orbital modulation defining the modulated component as the difference of the bright (Φ = 0.1 -0.4) and faint (Φ =0.7-0.9) phase UV continuum spectra. UV lines, except for the faint HeII emission at λ2386, have been removed by means of Gaussian fits to the 200 phase binned spectra.

Both a black-body and a power law ($F_\lambda \propto \lambda^{-\alpha}$) fits have been attempted yielding $T_{\rm eff}$ = 29200 ± 100 K (1 σ) ($\chi^2_{\rm red.}$ = 0.9) and a spectral index α = 1.62 ± 0.04 ($\chi^2_{\rm red.}$ = 0.7) respectively. This indicates that the UV modulation cannot be simply described by the tail of the hot ($\sim$ 15 eV (Rosen et al. 1996); $\sim$ 25 eV (Schwope et al. 1995)) black-body seen at higher energies. A similar conclusion was reached by Heise & Verbunt (1988) for AM Her. We note that the black-body does not satisfactoringly fit the near-UV part of the spectrum at $\lambda > 2000$ Å . A flatter distribution in the near-UV with respect to the far-UV range was also noted from IUE data (de Martino et al. 1995) and appears to be a common characteristic of mCVs (de Martino 1995), which in Polars is indicative of the accretion stream contribution.

A more quantitative description of the UV modulation has been derived by decomposing the observed bright and faint phase spectra into the contributions of the accretion heated white dwarf and the accretion stream. Due to the poor wavelength re-

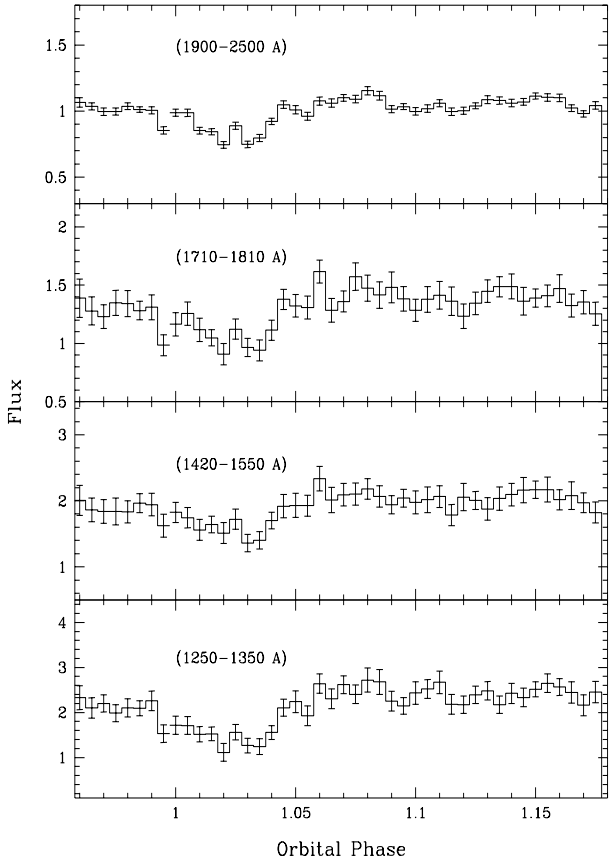

Fig. 4. The dip observed in the UV continuum light curves of QS Tel. Ordinates are in units of 10^{-14} erg cm^{-2} s^{-1} Å $^{-1}$.

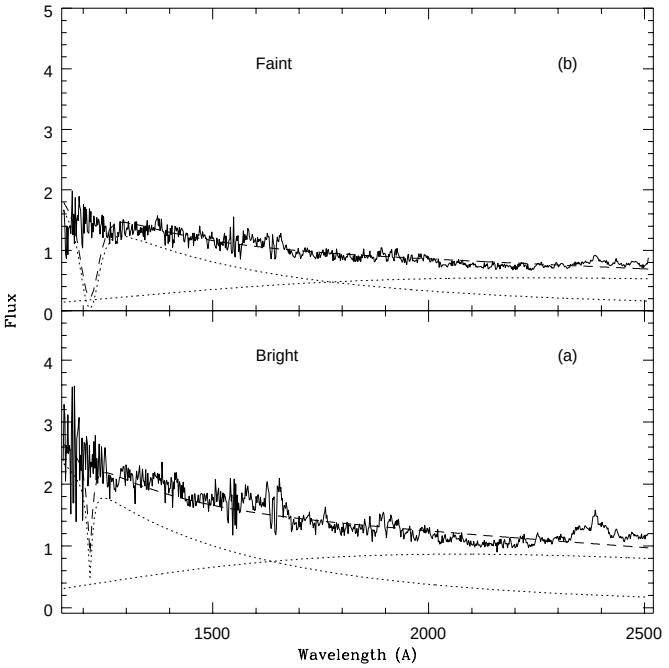

Fig. 5a and b. The bright (**a**) and faint (**b**) phase spectra (solid line) together with their best multicomponent fits accounting for the heated regions of the white dwarf and stream emissions (bright: T_{wd} = 45000K, $T_{str.}$=14000 K; faint: T_{wd}=24000 K, $T_{str.}$=15000 K). Each distribution is represented by a dotted line and the combined fitted spectra are represented by a dashed line. Fluxes are in units of 10^{-14} erg cm^{-2} s^{-1} Å $^{-1}$.

solution of our FOS spectra, the emissions of CIII, Lyα and NV overlap, we are unable to detect the photospheric Lyα absorption of the white dwarf and thus to set tight constraints on the temperature. Notwithstanding this, the observed UV continuum can be reasonably well described by white dwarf model spectra. We followed the procedure described by Gänsicke et al. (1995) using non magnetic pure-hydrogen line-blanketed white dwarf model spectra (log g =8.0) for the white dwarf emission and a black-body to account for an optically thick stream contribution. Temperatures of 45000 K ($\chi^2_{\rm red.}$ = 0.7) and 24000 K ($\chi^2_{\rm red.}$ = 0.5) are found for the bright and faint phase spectra, with corresponding sizes of $2{\cdot}10^8$ cm and $4{\cdot}10^8$ cm respectively for d=170pc. The derived black-body temperature and the emitting area for the accretion stream are very similar in both cases, $\sim$15000 K and $\sim 3 \cdot 10^{18}$ cm^2. Hence, during the bright phase, the hot, small core of the accretion heated region on the white dwarf dominates the UV emission, while we observe the cooler, larger "edge" of this region during the faint phase. Note that the derived radius of the emitting area is smaller than that of a white dwarf, indicating that the temperature of the underlying white dwarf is still lower and its emission is outshone by the accretion region. This picture is similar to the results for AM Her (Gänsicke et al. 1995). In Fig. 5, we show the bright (Fig. 5a) and faint (Fig. 5b) phase continuum spectra together with the fitted white dwarf and stream black-body contributions.

4.2.2. The dip spectrum

The dip continuum spectrum has been obtained by averaging the UV spectra between phases 0.0 and 0.05 and removing emission lines as described above. The presence of a turn-over in the far-UV, may be indicative of the contribution of the white dwarf photospheric Lyα absorption which, however, still appears to be masked. A composite white dwarf plus stream fitting (Fig. 6a.) gives T_{wd} = 19000 K, $R_{wd} = 7.1 \cdot 10^8$ cm with a stream temperature fixed at 15000 K ($\chi^2_{\rm red.}$ = 0.98). The emitting area of the stream is found to be $1.3 \cdot 10^{18}$ cm^2, lower than those derived during the bright and faint phases. Though the worse match is in the Lyα region, the dip spectrum reveals the cooler accretion region or even unheated white dwarf emission.

If the dip is produced by an occultation, its spectrum represents the contribution of the obscuring component plus the residual emission from the un-occulted component. On the other hand, the difference between the immediate out-of-dip and dip spectra may represent that of the occulted component (Fig. 6b). Note that the lines were not removed from the spectra before subtraction. The difference spectrum is remarkably characterized by the absence of emission lines except for a weak contribution from CIV due to radial velocity shifts in this phase range. The slope is very steep shortward $\sim$ 1500Å and spectral models other than a power law fail. We find a spectral index $\alpha = 4.9 \pm 0.3$ ($\chi^2_{\rm red.}$ = 0.4); no useful constraints on temperatures can be derived. The contribution of this hot component is

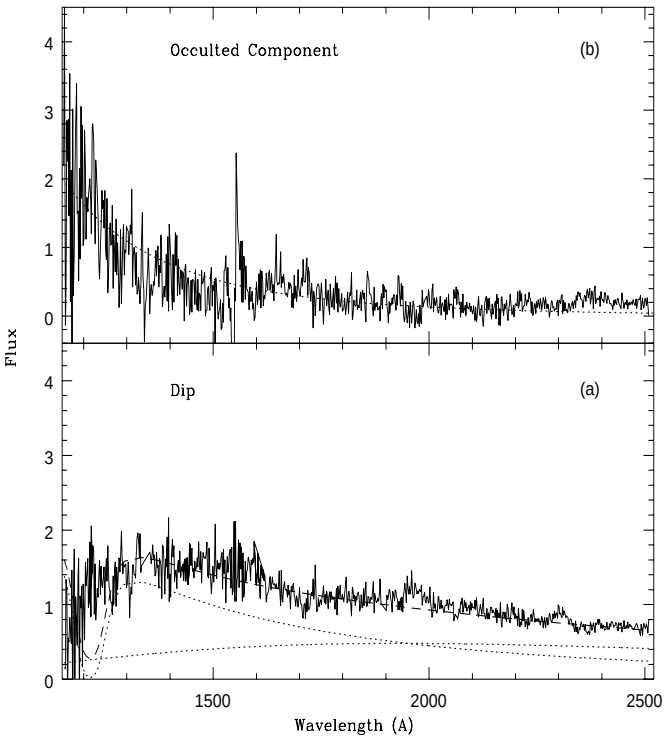

Fig. 6a and b. The dip continuum spectrum (**a**) together with the best fit (dashed line) white dwarf (T_{wd}=19000 K, R_{wd} = $7.1 \cdot 10^8$ cm) plus stream distribution fixed at 15000 K. Each distribution is represented by a dotted line. The occulted component (**b**) together with a $F_\lambda \propto \lambda^{-\alpha}$ distribution with α=4.9 (dotted line). Ordinates are in units of 10^{-14} erg cm^{-2} s^{-1} Å $^{-1}$.

$\sim$ 28% of the bright phase FOS flux. We further point out that its spectrum could be steeper if the dip is caused by absorption in material which is not opaque, since absorption is likely to be strongest at long wavelengths. When comparing the UV spectrum with that derived using the black-body model found from the orbitally averaged EUVE data by Rosen et al. (1996) (15 eV and $N_H = 4.3 \cdot 10^{19}$ cm^{-2}) we find that while the spectral shapes are roughly in agreement the latter overestimates the FOS flux by a factor of $\sim$ 2.5. Since the EUVE data where taken at a different epoch, we cannot gauge the importance of this discrepancy. In summary, the dip event allows us to infer the occultation of the hot, small EUV emitting core of the accretion heated region on the white dwarf.

4.2.3. The emission line behaviour

The orbital behaviour of the major UV lines, Lyα, NV, SiIV, CIV and HeII has also been investigated and their 200 bin phase flux light curves, except for the NV line, are presented in Fig. 3 (right side). These show a different modulation with respect to the continuum but similar to that observed with IUE (de Martino et al. 1995). The variations are not smooth with a broad roughly flat-topped maximum between phase 0.3 and 0.5 followed by a structured decay to a minimum between phase 0.0 and 0.1. Hence the line flux orbital maximum occurs later in phase than the continuum one. A plateau between phase 0.75 and 0.9 is also oberved as well as the short term ($\sim$ 10 min) flickering/flaring component as discussed in Sect. 4.1.

Furthermore, we do not recognize an obvious counterpart to the narrow continuum dip in the line flux variations. Although the observed minimum overlaps the continuum dip event, the morphology of the decrease of flux in this phase range is different. A noticeable exception is found for Lyα emission which is definitively absent in the phase range 0.96-0.1. The line variability is indeed strong with NV, SiIV, CIV and He II lines modulated by a factor of $\sim$ 3. The emission line ratios, NV/HeII, NV/SiIV, NV/CIV, are constant within errors as well as Lyα/HeII except in the dip phase range. This suggests that the bulk of these lines is formed in a common region. The observed behaviour in Lyα might be indicative of the line emission process as it will be discussed in Sect. 5.2.

We have also investigated the radial velocity behaviour of NV, SiIV, CIV and HeII using 20 phase bin averaged spectra. Each line has been fitted with a composite function consisting of Gaussians plus a linear polynomial for the local continuum. While for NV a single Gaussian has been used, for SiIV two were needed to account for the resonance components (λ 1393.76 and λ 1402.77). On the other hand, HeII and CIV emissions are better fitted with two Gaussians accounting for a broad and a "core" components. FWHMs of the broad component are $\sim$ 4000 km s^{-1} for HeII and $\sim$ 4500 km s^{-1} for CIV, while those of the "core" component are $\sim$ 1500 km s^{-1} for HeII and $\sim$ 1700 km s^{-1} for CIV. We also fixed a third broad (FWHM=40 Å) Gaussian at λ 1505 to account for the flat-field feature close to the CIV line, which prevents us to identify the blue hump seen in the IUE spectra. Although, the FWHM of the core component is of the same order of the resolution and then does not allow us to identify the so-called "narrow" component associated with the heated hemisphere of the secondary star, these FOS data give evidence that UV lines in QS Tel are structured.

Both SiIV components and NV line, as well as the core and broad components in CIV and HeII, show similar radial velocity behaviour with a maximum redshift at orbital phase $\sim$ 0.1 and a maximum blueshift at $\sim$ 0.6 in agreement with the IUE results. In Fig. 7 greyscale plots of the continuum subtracted 20 bin spectra in the regions around CIV (left side) and HeII (right side) are shown. The flat-field feature at λ 1505 was also removed. The broad and core components show similar amplitudes: 440 $\pm$ 30 km s^{-1} and 280 $\pm$ 45 km s^{-1} respectively. The quoted errors are to be considered as standard deviations from the mean of the two lines. We find a discrepancy in the γ velocities for the two components in each line: in CIV they differ from each other by -290 km s^{-1} while the difference is +40 km s^{-1} for HeII. This cannot be explained by the rest wavelengths used (1549.45 Å and 1640.4 Å respectively). But since γ velocities for HeII are similar to those found for the core and broad components in the Balmer lines (Rosen et al. 1996), we have some confidence in HeII results while we are careful with the CIV ones, as it is an unresolved doublet whose behaviour in the intensities with phase might introduce spurious effects.

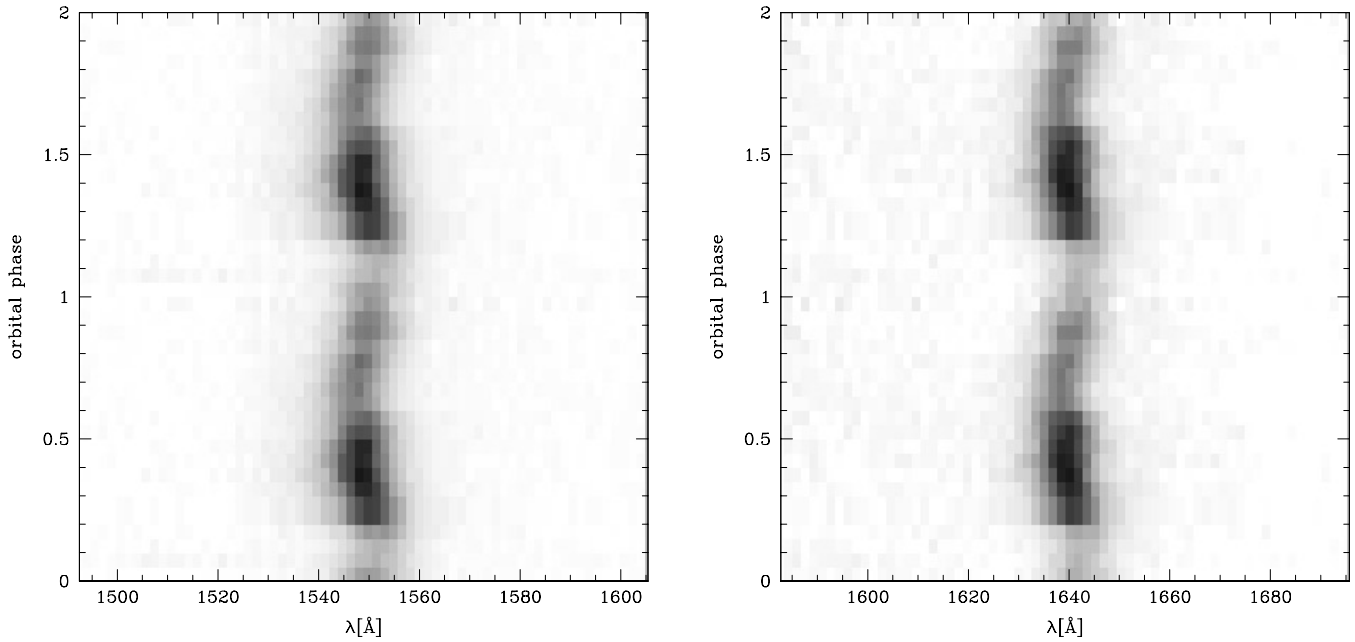

Fig. 7. Greyscale plot of the 20 binned continuum subtracted spectra in the spectral range around CIV (left) and HeII (right). The 0.9" aperture flat-field feature has also been removed. A broad and a "core" component are visible through the orbital cycle which is shown twice and with increasing phases from bottom to top.

5. Discussion and conclusions

The analysis presented so far has shown that the UV emission is composed of different contributions.

From a time series analysis we have found that the UV emission is dominated by the 140 min orbital variability. A flickering/flaring activity of the order of a few percent and on a timescale of a few minutes is also detected. This can be indicative of oscillation activity which appears to be present in mCVs with characteristic timescales ranging from few seconds to tens of minutes (Bonnet-Bidaud et al. 1991; Ramseyer et al. 1993; de Martino et al. 1994; Stockman & Schmidt 1996). While a few second oscillations can be due to thermal instabilities at the shock region above the white dwarf surface or at the Lagrangian point L1, longer scale variations might indicate instabilities in the accretion rate possibly in the form of blobs of material free-falling towards the white dwarf within the magnetospheric limit. We estimated 21 min and 29 min as upper limits to the free-fall times from the white dwarf magnetospheric radius for the two magnetic field strengths of 47MG and 70MG (Schwope et al. 1995) adopting an accretion rate of $2 \cdot 10^{17}$ g s^{-1} (Beuermann & Burwitz 1995), $M_{wd} = 0.6\ M_{\odot}$ and $R_{wd} = 7.1 \cdot 10^8$ cm (see below). The observed variations are well within these limits and hence could be indicative of material captured by the magnetosphere and tuned with a typical dynamical time inside the system.

The UV continuum orbital modulation has a single peaked quasi-sinusoidal shape, quite different from the light curves at higher energies when QS Tel was in a one pole accretion mode. The shape is also consistent with that observed with IUE when the system was independently found in a two pole accretion configuration by Rosen et al. (1996). Although we cannot exclude the contribution from a second emitting pole located at about the same azimuthal distance but in the opposite hemisphere, which will contribute with similar phasing, the morphology of the UV light curve suggest the presence of a dominant pole likely associated to the X-ray bright one. Also for AM Her only the main accreting pole was found to be bright in the UV (Gänsicke et al. 1995). However, the UV emitting heated region on the white dwarf surface has a complex structure and temperature distribution ranging from 45000 K and 24000 K. Another component, ascribed to the optically thick stream contribution, mainly detectable at longer wavelengths, accounts for $\sim 45\%$ of the total UV continuum during both bright and faint phases. The estimated temperature of ~ 15000 K is similar to those derived for the accretion stream in UZ For (Stockman & Schmidt 1996) and AM Her (Gänsicke et al. 1995).

The detection of a narrow dip in the continuum light curve, lasting 840 s, mostly in phase with that observed in the high energy light curves suggests that a relatively small region is involved. Its spectrum is consistent with two components: the stream, at approximately the same temperature as found during the bright and faint phases, and the emission from the unheated white dwarf (but also possibly the outer regions of the accretion heated spot) with an average temperature of 19000 K and size of $7.1 \cdot 10^8$ cm (d=170 pc). If we use this value as the white dwarf radius, then the fractional area of the heated white dwarf, ranges from $f \sim 0.08$ (faint phase) to 0.03 (bright phase), which is indeed very large when compared with the ~ 0.008 EUV spot (Rosen et al. 1996). Also for AM Her the heated white dwarf fractional area was found to be large ~ 0.1 (Gänsicke et al. 1995).

We note that the stream plus heated white dwarf contributions for the bright and faint phases at optical wavelengths yield to V=15.8 mag and 16.0 mag respectively, close to the observed high state magnitude of QS Tel. Also, the expected magnitude from the unheated white dwarf at 19000 K is V=17.5 mag, which is indeed observed when QS Tel enters into a low state.

An interesting result is the presence of a very hot component, likely the tail of the EUV black-body, mostly diluted by the contribution of the large heated white dwarf emitting area, which is eclipsed or occulted by the stream. This can be ascribed to the hottest parts of the polar cap.

The UV flux excess of the bright phase with respect to what we defined as the un-heated white dwarf is $F_{UV}=1.2\cdot10^{-12}$ erg cm^{-2} s^{-1}. We discuss this excess in terms of energy balance from the bright accreting primary X-ray pole. While the bremsstrahlung flux from this pole at orbital maximum was estimated to be $F_{Brems.}= 3\cdot10^{-13}$ erg cm^{-2} s^{-1} for kT=20 keV, the 25 eV black-body emission is $F_{BB}= 4.6 \pm0.3 \cdot 10^{-11}$ erg cm^{-2} s^{-1}, implying $F_{Brems.}/F_{BB} \sim 0.0065$ (Schwope et al. 1995). This fits into the general idea (Beuermann & Burwitz 1995) that the bremsstrahlung component is generally suppressed in presence of high magnetic fields. Hence if we ascribe the soft X-rays and UV flux to a reprocessed radiation, the cyclotron component should account for that. Using the cyclotron flux from the second high field faint X-ray pole $F_{cycl.} \sim 10^{-12}$ erg cm^{-2} s^{-1} (Schwope et al. 1995) as an estimate of the order of magnitude for the primary pole, we find that only the UV flux can be accounted for: $F_{UV} \approx F_{Brems.} + F_{cycl.}$. This implies that the soft X-ray emission does not enter into the energy balance and hence the reprocessing in the soft X-rays is mostly irrelevant and the flux comes from buried shocks (blobs penetrating the white dwarf surface). A similar result has been found for AM Her (Gänsicke et al. 1995).

QS Tel has been found in a high state, displaying strong UV emission lines whose luminosity is $1.4\cdot10^{31}$ erg s^{-1}. Resonance line ratios (NV/CIV, NV/SiIV and SiIV/CIV) are consistent with those observed in other Polars (de Martino 1995; Mauche et al. 1996). These lines are believed to arise from collisional excitation in a photoionized gas by hot radiation, although models still fail to explain the observed NV/CIV ratio (Mauche et al. 1996). As found from IUE data (de Martino et al. 1995), $\sim 4\%$ of the 25 eV black-body flux is intercepted and re-emitted in the UV lines.

The strong UV line orbital variability is not in phase with the continuum one: the maximum lags the continuum bright phase by ~ 0.2, except in the near-UV where they are mostly in phase. The radial velocity behaviour, with maximum red-shift when their flux is minimum and close to the time of the continuum dip, indicates that lines arise in common region(s) with similar kinematical properties. The broad and core components, the latter a mixture of unresolved contributions, detected in HeII and CIV also behave similarly. We then ascribe the UV line emitting region to the magnetically confined accretion stream towards the white dwarf.

No dip can be detected in the emission line light curves except for Lyα. Although we cannot precise the mechanism involved, a possible hypothesis is that during dip phases the accretion stream intercepts the UV flux from the white dwarf at Lyα energy. The emission from the stream is then compensated by absorption.

In conclusion, the analysis presented here has shown that UV observations with high temporal resolution may reveal new details in the accretion pattern as well as on the energy balance in Polars. Higher UV spectral resolution data are now indeed necessary to detect the different emission line components whose behaviour is mostly unexplored in this spectral range.

Acknowledgements. During part of this work DdM was under ESA contract and affiliated to the Astrophysic Division, Space Science Department at ESTEC.

References

Beuermann K. & Thomas H.-C., 1993, Adv. Space Res., 13,115.
Beuermann K. & Burwitz V., 1995, in *Cape Workshop on Magnetic Cataclysmic Variables*, eds. D.A.H. Buckley & B. Warner, ASP Conf. Ser. 85, p. 99.
Bonnet-Bidaud J.-M., Somova T.A. & Somov N.N., 1991, A&A,251, L27.
Buckley D.A.H., O'Donoghue D., Hassall B.J.M., Kellett B.J., Mason K.O., Sekiguchi K., Watson M.G., Wheatley P.J., Chen A., 1993, MNRAS 262, 93.
Cropper M., 1990, Space Science Reviews 54, 195.
Deeming T.J., 1975, Ap&SS,36,137.
de Martino D., Buckley D.A.H., Mouchet M., Mukai K., 1994, A&A 284, 125.
de Martino D., Buckley D.A.H., Mouchet M., Mukai K., 1995, A&A 298, L5.
de Martino D., 1995, in *Cape Workshop on Magnetic Cataclysmic Variables*, eds. D.A.H. Buckley & B. Warner, ASP Conf. Ser. 85, p. 238.
Eracleous M. & Horne K. 1996, ApJ 471, 427.
Gänsicke B.T., Beuermann, K. & de Martino, D., 1995, A&A, 303, 127.
Heise J. & Verbunt F., 1988, A&A 189, 112.
Kinney A.L. 1994, FOS Instrument Handbook, Space Telescope Science Institute, Version 5.0 (May 1994).
Keys C.D. 1995, FOS Instrument Handbook, Space Telescope Science Institute, Version 6.0 (June 1995).
Mauche C.W., Lee Y.P. & Kallman T.R., 1997, ApJ 477, 832.
Ramseyer T.F., Robinson E.L., Zhang E., Wood J.H., Stiening R.F. 1993, MNRAS 260, 209.
Roberts D.H., Lehar J., Dreher J.W. 1987, AJ, 93, 968.
Rosen S.R., Mittaz J.P.D., Buckley D.A.H., Layden A.C., Clayton K.L., McCain C., Wynn G.A., Sirk M.M., Osborne J.P., Watson M.G., 1996, MNRAS, 280, 1121.
Schwope A., Thomas H.-C., Beuermann K., Burwitz V., Jordan S., Haefner R., 1995, A&A, 293, 764.
Silber A.D., Anderson A.F., Margon B., Downes R.A., 1996, ApJ, 462, 428.
Stockman H.S. & Schmidt G.D., 1996, Ap.J., 468, 883.

This article was processed by the author using Springer-Verlag LaTeX A&A style file *L-AA* version 3.